Video Article

# Rapid Scan Electron Paramagnetic Resonance Opens New Avenues for Imaging Physiologically Important Parameters *In Vivo*

Joshua R. Biller[1,2], Deborah G. Mitchell[1], Mark Tseytlin[3,4], Hanan Elajaili[1], George A. Rinard[5], Richard W. Quine[6], Sandra S. Eaton[1], Gareth R. Eaton[1]

[1]Department of Chemistry and Biochemistry, University of Denver

[2]Magnetic Imaging Group, Applied Physics Division, Physical Measurements Laboratory, National Institute of Standards and Technology

[3]Department of Radiology, Geisel School of Medicine, Dartmouth University

[4]Department of Biochemistry, West Virginia University

[5]Department of Electrical and Computer Engineering, University of Denver

[6]Department of Engineering, University of Denver

Correspondence to: Gareth R. Eaton at gareth.eaton@du.edu

URL: https://www.jove.com/video/54068
DOI: doi:10.3791/54068

Keywords: Bioengineering, Issue 115, electron paramagnetic resonance (EPR), rapid scan, nitroxide, *in-vivo* imaging, 250 MHz, pH, oxygen concentration, redox status, signaling molecules, biophysics

Date Published: 9/26/2016

Citation: Biller, J.R., Mitchell, D.G., Tseytlin, M., Elajaili, H., Rinard, G.A., Quine, R.W., Eaton, S.S., Eaton, G.R. Rapid Scan Electron Paramagnetic Resonance Opens New Avenues for Imaging Physiologically Important Parameters *In Vivo*. *J. Vis. Exp.* (115), e54068, doi:10.3791/54068 (2016).

## Abstract

We demonstrate a superior method of 2D spectral-spatial imaging of stable radical reporter molecules at 250 MHz using rapid-scan electron-paramagnetic-resonance (RS-EPR), which can provide quantitative information under *in vivo* conditions on oxygen concentration, pH, redox status and concentration of signaling molecules (*i.e.,* $OH^{\bullet}$, $NO^{\bullet}$). The RS-EPR technique has a higher sensitivity, improved spatial resolution (1 mm), and shorter acquisition time in comparison to the standard continuous wave (CW) technique. A variety of phantom configurations have been tested, with spatial resolution varying from 1 to 6 mm, and spectral width of the reporter molecules ranging from 16 μT (160 mG) to 5 mT (50 G). A cross-loop bimodal resonator decouples excitation and detection, reducing the noise, while the rapid scan effect allows more power to be input to the spin system before saturation, increasing the EPR signal. This leads to a substantially higher signal-to-noise ratio than in conventional CW EPR experiments.

## Video Link

The video component of this article can be found at https://www.jove.com/video/54068/

## Introduction

Relative to other medical imaging modalities, electron paramagnetic resonance imaging (EPRI) is uniquely able to quantitatively image physiological properties including pH[1-3], $pO_2$[4-7], temperature[8], perfusion and viability of tissues[9], microviscosity and ease of diffusion of small molecules[10] and oxidative stress[11]. Estimation of the ease of disulfide cleavage by glutathione (GSH) in tissue and cells[12,13] can report on redox status. For *in vivo* imaging, EPR in the frequency range between 250 MHz and 1 GHz is chosen because these frequencies provide sufficient depth of tissue penetration (up to several cm) to generate images for small animals in which intensities are not diminished by dielectric loss effects. Higher frequencies, such as 9.5 GHz[14] (X-band) and 17 GHz ($K_u$-band)[15,16] can be used for imaging of skin and hair or single cells, respectively. The success of EPRI at all frequencies depends on paramagnetic spin probes that are specific for tissues so that their location and fate may be imaged.

If the environment of an electron spin probe is spatially heterogeneous, the EPR spectrum is the sum of contributions from all locations. Spectral-spatial imaging divides the sample's volume into an array of small spatial segments and calculates the EPR spectrum for each of these segments[17]. This allows mapping of the local environment by measuring the spatial variation in the EPR spectrum. Magnetic field gradients are used to encode spatial information into EPR spectra, which are called projections. The spectral-spatial image is reconstructed from these projections[18,19].

In RS-EPR the magnetic field is scanned through resonance in a time that is short relative to electron spin relaxation times (**Figure 2**)[20,21]. Deconvolution of the rapid-scan signal gives the absorption spectrum, which is equivalent to the first integral of the conventional first-derivative CW spectrum. The rapid-scan signal is detected in quadrature, so that both absorption and dispersion components of the spin system response are measured. This is essentially collecting twice the amount of data per unit time. Saturation of the signal in a rapid scan experiment happens at higher powers than for CW, so higher powers can be used without concern for saturation.[20,22] Many more averages can be done per unit time in comparison to CW. Higher power, direct quadrature detection and more averages per unit time combine to give rapid scan a better signal-to-

 

noise ratio (SNR), especially at high gradient projections that define spatial separation, leading to higher quality images. To achieve about the same SNR for an image of a phantom required about 10 times as long for CW as for rapid scan[23].

The increased SNR also allows experiments at 250 MHz with low concentration spin trap adducts formed by the reaction of OH with 5-tert-butoxycarbonyl-5-methyl-1-pyrroline-*N*-oxide (BMPO-OH) which would be invisible to the CW method[24]. Dinitroxides connected with a disulfide linker are sensitive to cleavage by glutathione, and so can report on cellular redox status. Equilibrium exists, dependent on the concentration of glutathione present, between the di- and mono-radical forms. Observing these changes requires capture of the entire 5 mT wide spectrum, and can be achieved much faster with rapid scan EPR compared to stepping the magnetic field in a CW experiment.

A complete rapid scan system consists of four parts: the spectrometer, the main field magnet, the rapid scan coil driver, and the rapid scan cross-loop resonator. The spectrometer and the main field magnet function the same as in a CW experiment, setting the main Zeeman field and collecting the data from the resonator. The rapid scan coil driver generates the sinusoidal scan current that goes into specially designed rapid scan coils on the rapid scan cross-loop resonator. The rapid scan coils on the rapid scan cross-loop resonator generate a large homogeneous magnetic field, which is swept at frequencies between 3 and 15 kHz.

## Protocol

# 1. Setup of the Rapid Scan Coil Driver at 250 MHz

1. **Calculation of Rapid Scan Experimental Conditions**
   Note: The most important parameter in RS-EPR is scan rate, α, which is the product of scan frequency and scan width (Equation 3). For narrow scan widths, faster scan rates are used, and for wider sweep widths, slower scan rates are used. The following instructions step through the latter case and show how to arrive at the experimental coil driver parameters of 7 mT sweep width and 6.8 kHz scan frequency.
   1. Determine the resonator bandwidth ($BW_{Res}$).
      $$BW_{Res} = \frac{\nu_{res}}{2Q} = \frac{250\ MHz}{180} = 1.39\ MHz \quad (1)$$
      where $\nu_{res}$ is the operating frequency of the resonator and *Q* is the quality factor. Q = 90, is common for the rapid scan resonator used to obtain the data in Representative Results.
   2. Determine the rapid scan rate, *α*, allowed by the resonator bandwidth $\alpha = \frac{\sqrt{3}\pi\Delta B_{pp} BW_{Res}}{N}$ (2)
      $$\alpha = \frac{\sqrt{3}\pi(0.1\ mT)(1.39\ MHz)}{5} = 150\ T/s$$
      where *N* is a constant often conservatively selected to be 5-6, $\Delta B_{pp}$ is the peak-to-peak derivative linewidth in mT, and *a* is the scan rate if T/s for a Lorentzian linewidth.
      Note: A common value for the radicals in the representative section is $\Delta B_{pp}$ = 0.1 mT. In comparison with earlier rapid scan literature; Equation 2 is derived by setting the signal bandwidth ($BW_{sig}$) equal to $BW_{Res}$.
   3. Determine the maximum rapid scan frequency allowed by the rate.
      $a = \pi w f$ (3)
      $150\ T/s = \pi(7\ mT)f$
      where *w* is the width of the scan and *f* is the scan frequency. A sweep width of 7 mT will cover 100% of the spectrum for current probes used *in vivo*. Use this value and the rate calculated in (Equation 2) to determine the scan frequency.
      $$f = \frac{150\ T/s}{\pi(7\ mT)} = 6.8\ kHz$$

2. **Selection of tuning capacitors and tuning of rapid scan coil driver**
   Note: The rapid scan coil driver is typically run in a resonated mode generating a sinusoidal wave. Resonance occurs at a scan frequency where the inductive and capacitive reactances are of equal magnitude and opposite signs, so that total reactance is close to zero.
   1. Determine the proper capacitance for the frequency determined in 1.1.3 using the inductance, *L*, of the rapid scan coils and (Equation 4).
      $$C_{TOT} = \frac{1}{L(2\pi f)^2} \quad (4)$$
      $$C_{TOT} = \frac{1}{4.9\ mH(2\pi 6.8\ kHz)^2} = 4.8\ mF$$
   2. Divide $C_{TOT}$ from (Equation 4) in half to get the capacitor values for each side of the coil driver capacitor box.
      $$C_1 = C_2 = \frac{C_{TOT}}{2} \quad (5)$$
      $$C_1 = C_2 = \frac{4.8\ mF}{2} = 2.4\ mF$$
      Note: The rapid scan coil driver has two amplifiers. When selecting a capacitor, the capacitor box needs to be balanced with an equal capacitance on each side of the box. The two sides are in series.
   3. Unscrew the top cover of capacitor box and insert capacitors on both sides that are equal to the value determined in step 1.2.2.
   4. Replace the top of the capacitor box and screw it down to ensure it stays on.
   5. Using the front panel of the resonated coil driver, adjust the output frequency until the sinusoidal waveform has the maximum amplitude.

## 2. Preparation of Reagents and Phantoms

1. **Preparation of radicals**
    1. Remove $^{15}$N-PDT from the freezer and allow the container to come to room temperature (10-15 min).
    2. Weigh out 1.4 mg of $^{15}$N-PDT using an analytical balance.
    3. Add 1.4 mg of $^{15}$N-PDT to 15 ml de-ionized (DI) $H_2O$ for a final concentration of 0.5 mM.
    Note: 4-oxo-2,2,6,6-tetra($^2H_3$)methyl-1-(3,3,5,5-$^2H_4$,1-$^{15}$N)piperdinyloxyl ($^{15}$N-PDT), 4-$^1$H-3-carbamoyl-2,2,5,5-tetra($^2H_3$)methyl-3-pyrrolinyloxyl ($^{15}$N-mHCTPO) and 3-carboxy-2,2,5,5-tetra($^2H_3$)methyl-1-(3,4,4-$^2H_3$,1-$^{15}$N)pyrrolidinyloxy ($^{15}$N-Proxyl)[25] (**Figure 1E-G**) radicals have long term stability (2 years) in aqueous solution and at room temperature. Their solid forms are usually stored in a freezer or refrigerator to keep these radicals stable for years. The stability of nitroxide radicals generally make them non-toxic, and their preparation can be done on a normal benchtop when the solvent is water. When using organic solvents, prepare nitroxide solutions inside a fume hood while outfitted with the proper personal protective equipment (PPE).

2. **Preparation of pH sensitive trityl radicals**
    1. Weigh out 0.7 mg of triaryl methyl radical ($aTAM_4$)[26] radical (1,400 g/mol) and dissolve in 200 µl of absolute ethanol.
    2. Weigh 0.00681 g of $KH_2PO_4$ (136.1 g/mol) and dissolve in 50 ml DI water for a final concentration of 1 mM.
    3. Weigh 2.8 g of KOH (56 g/mol) and dissolve in 50 ml of DI water for a final concentration of 1 M.
    4. Add KOH drop wise to the phosphate buffer (2.2.2) to adjust the pH of 7.0.
    5. Add 800 µl of 1 mM phosphate buffer and the 200 µl of $aTAM_4$ in absolute ethanol for a final concentration of 0.5 mM in 80:20 buffer:ethanol.
    6. Repeat steps 2.2.1-2.2.5 to create the $aTAM_4$ sample at pH = 7.2.
    7. Place the $aTAM_4$, pH=7.0 and $aTAM_4$, pH=7.2 into separate 6 mm quartz sample tubes.
    8. Place both 6 mm quartz EPR tubes into a 16 mm quartz EPR tube, with a 2 mm thick Styrofoam spacer in between.
    Note: The walls of the quartz sample tube are 0.5 mm thick, and in addition to the 2 mm spacer yield a 3 mm separation between the aTAM samples. The pH sensitive trityl radicals used were synthesized at the Ohio State University[26]. The example that was used for imaging is called $aTAM_4$. The reaction which accounts for the pH sensitivity is shown in **Figure 1A**.

3. **Generation of BMPO-OH**
    1. Weigh out 680 mg of $KH_2PO_4$ and dissolve in 100 ml DI water for a final concentration of 50 mM.
    2. Add 1 M KOH drop wise to the phosphate buffer to pH=7.3.
    3. Weigh out 50 mg of BMPO (199.25 g/mol).
    4. Combine the 50 mg of BMPO with 5 ml of phosphate buffer in a 16 mm quartz irradiation tube.
    5. Add 100 µl of 300 mM hydrogen peroxide.
    6. Irradiate the mixture in the 16 mm quartz irradiation tube with a medium pressure 450 W UV lamp for 5 min.
    7. Using a glass transfer pipet, transfer 2.5 ml of irradiated BMPO-OH solution out of the quartz irradiation tube and into one side of a 16 mm quartz sample tube with 3 mm divider.
    8. Transfer the remaining 2.5 ml of irradiated BMPO-OH into the other side of the 16 mm quartz sample tube with 3 mm divider.

4. **Preparation of dinitroxide radical**
    1. Weigh out 24.7 mg of $^2$H,$^{15}$N-disulfide dinitroxide (**Figure 1C**) in 1 ml DMSO for a stock solution of 47.5 mM.
    2. Prepare 10 mM Tris buffer and adjust to pH 7.2.
    3. Take 40 µl dinitroxide stock solution and dilute with Tris buffer to a final concentration of 1 mM.
    4. Place 250 µl of dinitroxide solution in buffer in a 16 mm quartz sample tube with a 10 mm divider in the center.
    5. Weigh out 154 mg of glutathione and add to 5 ml of Tris buffer for a final concentration of 100 mM.
    6. Add 5 µl of the 100 mM glutathione solution to 250 µl of 1 mM dinitroxide solution on one side of the 10 mm divider to convert the diradical into monoradical.

5. **Preparation of nitronyl nitroxide**
    1. Remove the radical from the freezer and allow the container to come to room temperature (10-15 min).
    2. Weigh out 1.9 mg of nitronyl (390 g/mol).
    3. Weigh out 0.56 mg of KOH and dissolve in 10 ml DI water for a final concentration of 1 mM.
    4. Mix the 1.9 mg of nitronyl into 10 ml of 1 mM KOH solution for a final concentration of 0.5 mM nitronyl.
    Note: If necessary, use a vortexer or sonicator to speed solvation of the nitronyl.

## 3. Setup of the Rapid Scan Instrument at 250 MHz

Note: Tuning of the resonator with an aqueous sample of nitroxide radical, which has a similar effect on resonator Q and tuning as buffer solution, is a good way to set up for the sample to be imaged

1. **Tune the resonator with an aqueous sample of nitroxide radical.**
    1. Insert the 15 ml of 0.5 mM $^{15}$N-PDT in water sample into a 16 mm quartz EPR tube.
    2. Insert the quartz tube into the detection side of the cross-loop RS-EPR resonator.
    3. Change the frequency of the instrument source until it matches the frequency of the detection side that contains the sample. Manually change the carrier frequency of the 250 MHz source by entering the desired value in software.
    4. Change the frequency of the excitation side to match the frequencies of the experiment source and detection side of the resonator. Change the frequency of the excitation side by turning a variable capacitor within the resonator cavity according to manufacturer's protocol.

2. **Set up Instrument Console and Main Magnet**
    1. Turn on the spectrometer and choose an experiment which records transient data with time on the abscissa.
    2. Within the software, set the number of points to 65,536 and the time base to 10 nsec.
    3. Set the number of averages to 10,000 for a strong or narrow signal, and to 45,000 for a broad or weak signal.
    4. Press the "engage" button in the software to send the experimental parameters from the software to the console and energize the main field magnet.
    5. Set the main magnetic field to 9 mT.
    6. Set the power attenuation knob to 50 dB, and turn on the 7 W high power amplifier.

## 4. Execution of Rapid Scan Experiment

Note: Specific instructions related to analysis of phantoms containing BMPO-OH[24], pH sensitive TAM radicals[19,27] and redox sensitive dinitroxides[28] are provided in the literature.

1. **Power saturation of standard nitroxide sample**
   Note: It is advantageous to do a power saturation curve on a standard nitroxide radical sample under the same experimental conditions which will be used to look at radicals sensitive to pH or redox status.
    1. Turn on the rapid scan coil driver, with the values from Section 1 (scan frequency of 6.8 kHz and scan width of 7 mT).
    2. Starting at 50 dB, collect a rapid scan spectrum with 100k averages. Decrease the attenuation by 3 dB and repeat the measurement. Continue until an attenuator setting of 0 dB, or for as long as the isolation measurement on the bridge readout is < 0.
    3. Transfer the raw rapid scan data into a deconvolution program (for example written in Matlab) and process the raw data into the absorption spectrum.
    4. Enter the scan frequency, sweep width, number of points and timebase into the program, and run the program to process the raw rapid scan signal into an absorption signal.
    5. Plot the amplitude of the absorption signal as a function of the square root power (in Watt) incident on the resonator. In the non-saturating regime, the amplitude is linearly dependent on the square root of the incident power.
    6. Fit a trend line starting at 0,0 and include all data points which fall into the linear response region. In the linear response region, signal amplitude increases proportional to the square root of microwave power.
    7. Extrapolate this trend to higher powers, and compare the EPR signal intensity. Use the highest power for which the signal amplitude does not deviate more than 3% from the extrapolated trend line. In order for the deconvolution of the rapid scan signal to work properly, the signal must still be in the linear response region with respect to incident power.
       Note: Transfer of the raw rapid scan data can be done over a network connection or via thumb drive. In this case the transfer is necessary because the program to process raw data (Matlab) is not on the same computer which has data collection software. The deconvolution algorithm which processes raw data is described in [29].

## Representative Results

The product of the experiment is a set of projections that are reconstructed into two-dimensional (one spectral, one spatial) images with a false color scale to represent signal amplitude. Deep blue denotes baseline where no signal is present, green is low amplitude and red is highest. Slices along the x-axis (spectral dimension) depict the EPR signal (EPR transition) on a magnetic field axis. Along the y-axis (spatial dimension), separation between signals corresponds to the physical spatial separation between samples in the resonators.

**Figure 3** shows a comparison of two images, acquired with CW (**Figure 3B**) or RS (**Figure 3A**) of a phantom with three different types of $^{15}$N substituted nitroxide radicals (**Figure 3D**). The broadest signal corresponds to $^{15}$N-Proxyl, a five member pyrrolidine ring with a negative charge at physiological pH, which could help target the molecule to specific cellular compartments. The doublet signal belongs to $^{15}$N-mHCTPO and is the result of a single hydrogen amidst otherwise complete deuteration. This single splitting has been optimized to monitor changes in oxygen concentration[30]. The narrowest signal comes from $^{15}$N-PDT, a flexible piperidine ring that is completely deuterated. It can be used to monitor oxygen concentration, or redox environment (reduction of the structure leads to decrease in EPR signal).

For the same 5-min acquisition time, the RS image shows superior spatial resolution and clarity of the spectral pattern for each radical. One reason for the improvement of RS over CW can be seen by comparing spectra at two different gradient strengths between the two techniques (**Figure 3C**). As the gradient strength increases the spectral signal is broadened. Considerable degradation of the CW spectrum under the high gradients (1 mT/cm) which encode spatial information.

Because a derivative signal broadens more quickly than an absorption signal, the SNR for the highest gradient CW projection (red trace) is very poor compared to that of the highest gradient RS projection (blue trace). Linewidth as a function of spatial position can be extracted from a 2D plot. Linewidth will be broad or narrow based on changes in oxygen concentration or viscosity around the nitroxide probe. The phantom imaged in **Figure 3A** was at room temperature and open to the air. Since oxygen content and viscosity (as determined by temperature) remained steady, the linewidth of each probe should be constant across the width of each tube containing a radical. **Figure 4** shows the scatter in linewidths fit from slices through the 2D image compared to the true linewidth value (black horizontal line). The image slice values, especially for $^{15}$N-PDT, are a better match to the true linewidth value for RS (**Figure 4A**) than for CW (**Figure 4B**). This is also a result of the improved SNR of RS over the CW technique.

Another benefit of the RS technique is the ability to generate wide magnetic homogeneous field sweeps in a very short time. A typical scan frequency for experiments at 250 MHz is 9 kHz, corresponding to 0.11 msec. This is 0.11 msec whether the field sweep is 0.5 mT or 5.0 mT. Compare this to CW, where a 5.0 mT sweep will take tens of seconds to minutes. With rapid scan it becomes possible to *quickly* collect 100% of the spectral information in times which are amenable to *in vivo* imaging.

**Figure 5** demonstrate wide spectrum RS-EPR imaging applied to spin trapping models. Important signaling molecules, like $OH^{\bullet}$ and $NO^{\bullet}$ are endogenous free radicals with very short lifetimes. In order to study these molecules, "spin traps" are used. An example of the reaction of spin trap [31] (BMPO) with $OH^{\bullet}$ is shown in **Figure 1B**. Imaging of a phantom containing 5 μM BMPO-OH adduct is shown in **Figure 5** (**A**, **B**). The spin-trap adduct signal is dependent on the starting concentration of $OH^{\bullet}$ and has a half-life of 30 minutes allowing study of any processes which generate $OH^{\bullet}$. The nitronyl nitoxide[32] was used as another example of wide spectrum imaging, but has been used in the past for spin-trapping of $NO^{\bullet}$[33,34]. Imaging of a phantom containing nitronyl is shown in **Figure 5** (**C**, **D**). For spin traps, capturing the entire spectrum allows better designation of the original transient radical species that was present.

Sensitivity to physiological changes like pH and redox status is derived from changes in the entire spectrum. **Figure 6** shows imaging with $aTAM_4$. In **Figure 6B**, the profile of $aTAM_4$ at pH= 7.0 (blue) has many spectral features, and a slice from the image matches well with the corresponding zero gradient spectrum (green). Compare this to the profile of $aTAM_4$ at pH=7.4, **Figure 6C**, with fewer spectral features and still in good agreement with the corresponding zero gradient spectrum. Imaging of phantoms containing of the dinitroxide in its dimeric, and reduced monomeric form are shown in **Figure 7**. The two different spectra are generated by cleavage of a disulfide (S-S), and so convey sensitivity to redox environment[1,35].

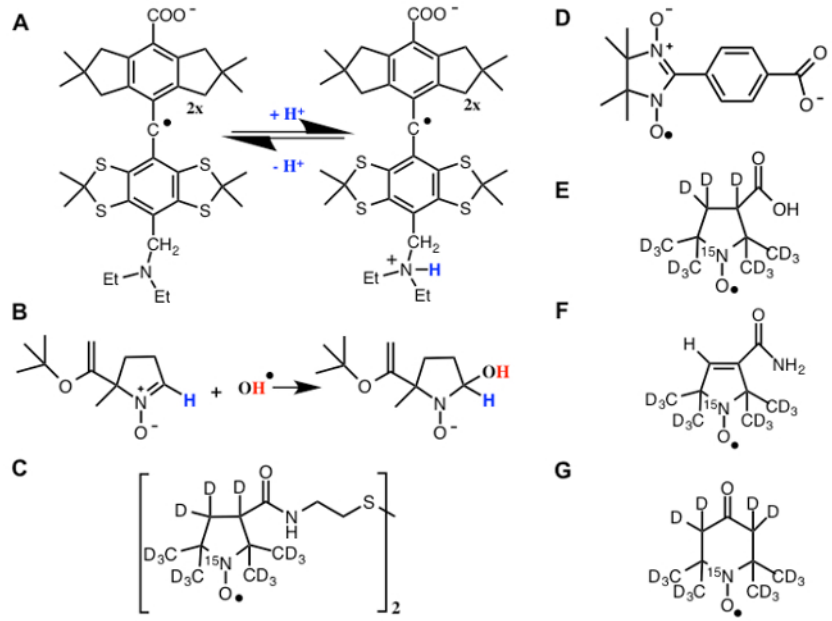


**Figure 1. EPR probes are sensitive to many physiological changes.** (**A**) An example of the pH-sensitive tri-aryl-methyl (TAM) radicals[26]. (**B**) Spin trap BMPO. (**C**) $^{15}$N-dinitroxide. (**D**) The nitronyl. (**E**) $^{15}$N-Proxyl. (**F**) $^{15}$N-mHCTPO. (**G**) $^{15}$N-PDT. Please click here to view a larger version of this figure.

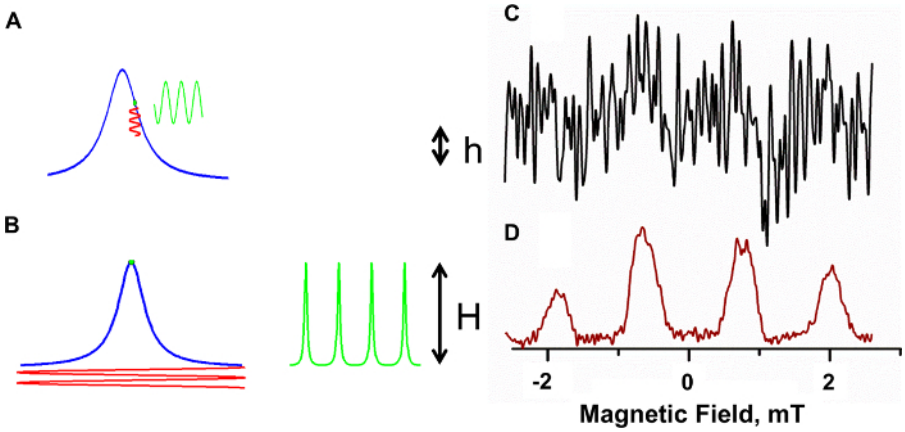


**Figure 2. Rapid scan EPR has inherently better SNR.** (**A**) In CW EPR the amplitude **h** is a small fraction of the total signal, determined by the magnetic field modulation. (**B**) In direct-detected rapid scan, the full signal amplitude is detected. The signal to noise increase is evident in the experiment where superoxide generated by *E. faecalis* is trapped with BMPO at X-band. For the same 30 sec acquisition time, hardly any signal is observable in the CW spectrum (**C**) while a strong signal is observed in the rapid scan spectrum (**D**)[36]. Please click here to view a larger version of this figure.

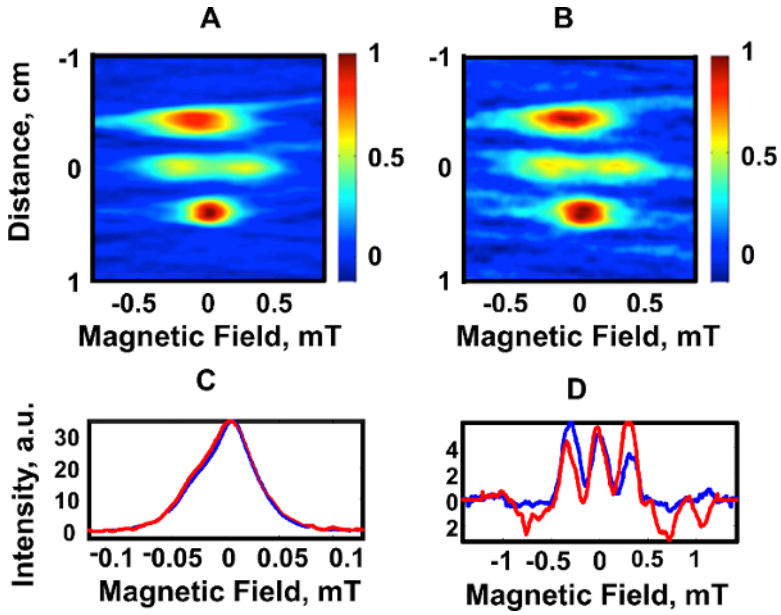


**Figure 3. Improved SNR allows better spatial resolution.** For the same 5-minute acquisition time, the RS image (**A**) has better SNR and spatial resolution compared to the one acquired with CW (**B**). (**C**) There is good agreement between projections acquired with rapid scan (blue) and CW (red) when no gradient is present (0 mT/cm) (**D**). Please click here to view a larger version of this figure.

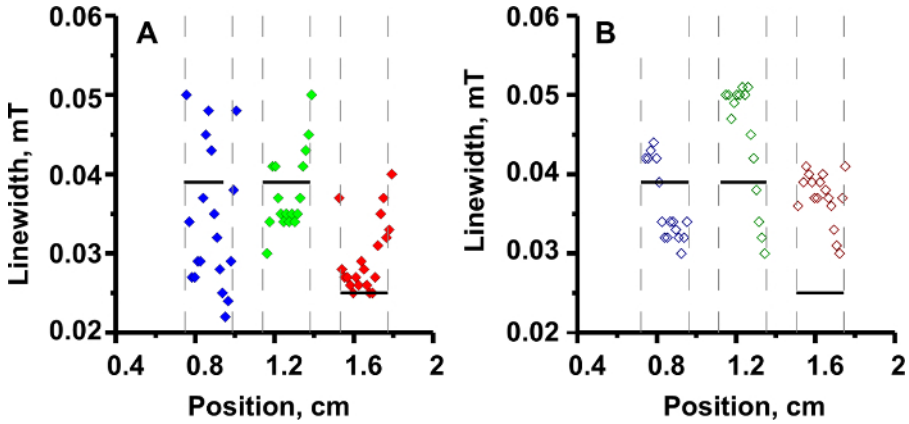


**Figure 4. The information content of a rapid scan image is higher than for CW.** (**A**) Slices of the 2D RS image. (**B**) Slices of the 2D CW image. The true linewidth (black horizontal line) of each sample is shown for comparison. See reference[23]. Please click here to view a larger version of this figure.

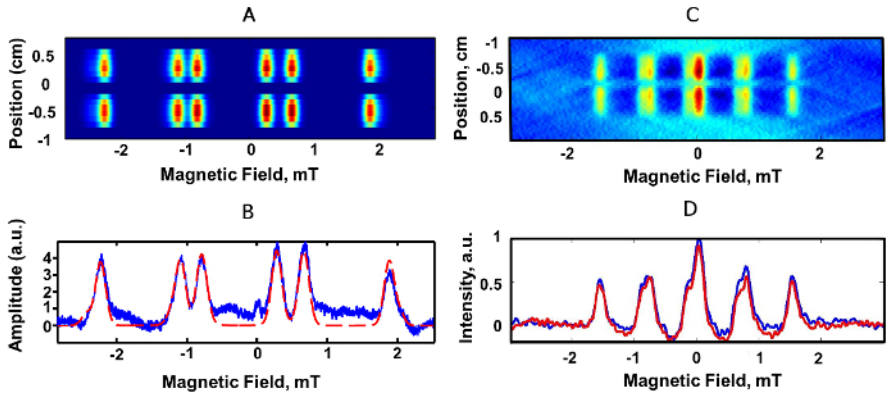


**Figure 5. Rapid field sweeping allows capture of an entire spectrum in a few seconds.** (**A**) 2D spectral-spatial image of a phantom consisting of BMPO-OH adduct. (**B**) A simulation fit to the zero-gradient BMPO-OH spectrum at 250 MHz was used to fit the initial BMPO-OH image and distinguish between regions containing BMPO-OH and noise containing regions. (**C**) $^{14}$N nitronyl radical which can be used for the trapping of nitric oxide *in vivo*. (**D**) Slices through each spectrum show the spectral shape at 250 MHz. See reference[19]. Please click here to view a larger version of this figure.

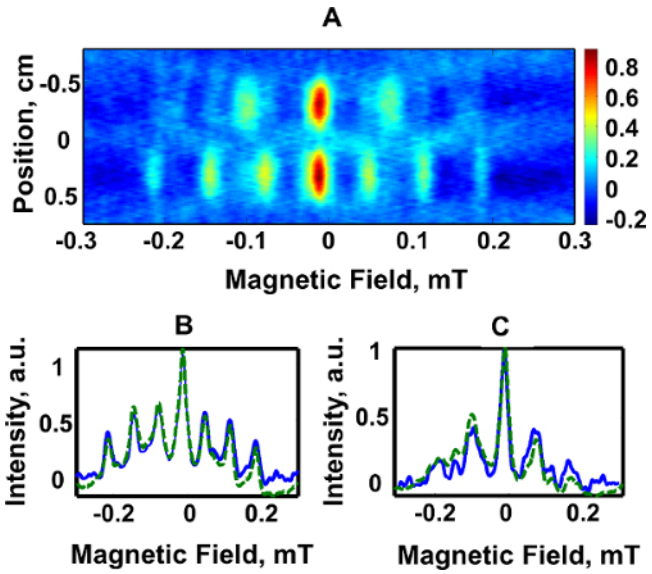


**Figure 6. No part of the spectrum is left out, allowing better monitoring of physiologically induced spectral changes.** (**A**) 2D spectral-spatial image of a phantom consisting of two tubes of pH sensitive $aTAM_4$ radical. (**B**) Spectral profile of $aTAM_4$ at pH= 7.0 (blue) and the corresponding zero gradient spectrum (green). (**C**) Spectral profile of $aTAM_4$ at pH=7.4 B (blue) and the corresponding zero-gradient spectrum (green). See references[19,26,37]. Please click here to view a larger version of this figure.

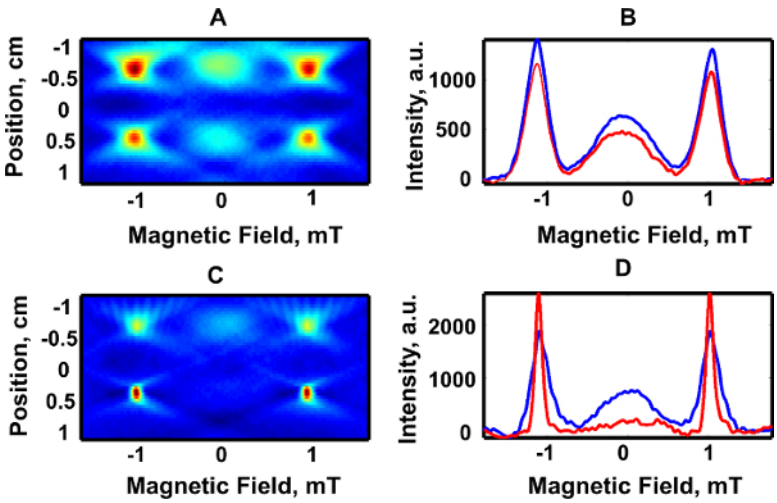


**Figure 7. Rapid scan opens the door to *in vivo* redox monitoring at 250 MHz.** (**A**) 2D spectral-spatial images of $^{15}$N-dinitroxide. (**B**) Slices through top (blue trace) and bottom (red trace) compartments in the two images. (**C**) The top compartment remains the same, but the bottom compartment has been reduced with glutathione. (**D**) Slice through each image object showing the change in the 1D spectrum of the bottom compartment. See references[1,28,35]. Please click here to view a larger version of this figure.

## Discussion

Rapid-scan signals have higher frequency components than CW, and require a larger resonator bandwidth depending on linewidths, relaxation times, and the speed of the rapid-scans. The bandwidth required for a given experiment is based upon the linewidth and the scan rate of the magnetic field (Equation 2). Depending on the relaxation times of the probe under study ($T_2$ and $T_2$*), and the scan rate, oscillations can appear on the trailing edge of the signal. For nitroxide radicals with $T_2$ ~500 nsec at 250 MHz (57$^{th}$ Rocky Mountain Conference on Magnetic Resonance, Epel, B, *et al.*, 2015), experimental scan rates are often not high enough to observe any oscillations.

The experimental bandwidth is typically limited by the resonator bandwidth. Each half cycle of a rapid scan experiment is recorded with either decreasing or increasing field/frequency, so the experimental bandwidth is ½ the resonator bandwidth, as shown in (Equation 1). If the experimental bandwidth is limited by the choice of parameters such that it is greater than resonator bandwidth and oscillations are damped, broadening results in the deconvolved line. Since the experiment bandwidth is determined by the rate and linewidth of the radical being studied, understanding these features is a key component of the rapid scan experiment.

The current protocol demonstrates EPRI at 250 MHz of phantoms containing probes sensitive to oxygen, viscosity, pH, endogenous transient signaling molecules (*i.e.*, $OH^{\bullet}$, $NO^{\bullet}$) and redox status. Spatial resolutions between 1 and 3 mm have been demonstrated, with experimental acquisition times between 29 seconds (single line of a 2 line $^{15}$N spectrum, **Figure 3**) and 15 minutes (full spectrum of 5 µM BMPO-OH, **Figure**

**5**). Method development with the phantoms shows use of RS-EPR images supersedes the conventional CW-EPR imaging technique[23,24], and opens new avenues for *in vivo* imaging using EPR probes.

EPRI is advantageous over other *in vivo* imaging techniques based on fluorescence or phosphorescence, as EPR probes are sensitive to a wider variety of *in vivo* phenomena. In addition, RF penetration at 250 MHz is ~7 cm, so that anomalous tissue at a deeper level can be studied. Nuclear magnetic resonance imaging (MRI) provides very detailed anatomical maps, but struggles to provide quantitative physiological information. A combination of MRI and EPRI could one day result in an all magnetic resonance version of a positron-emission-tomography (PET)/computed tomography (CT) scanner. Such an instrument would provide the same benefit of PET/CT, but without the heavy radiation doses or expensive radio-tracers.

Method development with phantoms continues to push the limits of RS-EPR, but the ultimate goal is to implement the technique in laboratories using animal models. Calculations for image reconstructions will need to be improved to speed data collection for a 4D experiment (3 spatial, 1 spectral dimension). An improved algorithm is currently being developed and is essential for *in vivo* applications, however the proof of principle may be done with 2D imaging.

Many of the radicals, such as $^{15}$N-PDT, used in phantoms degrade quickly under *in vivo* conditions with half-lives of only 60 seconds. Radicals with an improved resistance to *in vivo* reduction[39] have been synthesized and are important for building large enough concentrations *in vivo*. The enhanced sensitivity of RS-EPR over CW-EPR[24] will be another benefit in solving this problem. The sensitivity of rapid scan is currently 5 μM for a phantom, and between 100 μM and 5 mM, depending on the probe to be imaged, for animal studies being performed at the University of Chicago (personal communication, Maggio, M., 2015). The RS method will continue to be developed to close this gap, but the application has already begun to move into actual *in vivo* applications (57$^{th}$ Rocky Mountain Conference on Magnetic Resonance, Epel, B, *et al.*, 2015).

## Disclosures

We have nothing to disclose.

## Acknowledgements

Partial support of this work by NIH grants NIBIB EB002807 and CA177744 (GRE and SSE) and P41 EB002034 to GRE, Howard J. Halpern, PI, and by the University of Denver is gratefully acknowledged. Mark Tseytlin was supported by NIH R21 EB022775, NIH K25 EB016040, NIH/NIGMS U54GM104942. The authors are grateful to Valery Khramtsov, now at the University of West Virginia, and Illirian Dhimitruka at the Ohio State University for synthesis of the pH sensitive TAM radicals, and to Gerald Rosen and Joseph Kao at the University of Maryland for synthesis of the mHCTPO, proxyl, BMPO and nitronyl radicals.

## References

1. Bobko, A. A. *et al.* In vivo monitoring of pH, redox status, and glutathione using L-band EPR for assessment of therapeutic effectiveness in solid tumors. *Magn. Reson. Med.* **67** (6), 1827-1836 (2012).
2. Utsumi, H. *et al.* Simultaneous molecular imaging of redox reactions monitored by overhauser-enhanced MRI with 14N-and 15N-labeled nitroxyl radicals. *Proc. Nat. Acad. Sci. U.S.A.* **103** (5), 1463-1468 (2006).
3. Khramtsov, V. V., Grigor'ev, I. A., Foster, M. A., Lurie, D. J., & Nicholson, I. Biological applications of spin pH probes. *Cell. Mol. Bio.* **46** (8), 1361-1374 (2000).
4. Halpern, H. J. *et al.* Oxymetry Deep in Tissues with Low-Frequency Electron-Paramagnetic Resonance. *Proc. Nat. Acad. Sci. U.S.A.* **91** (26), 13047-13051 (1994).
5. Matsumoto, S. *et al.* Low-field paramagnetic resonance imaging of tumor oxygenation and glycolytic activity in mice. *J. Clin. Invest.* **118** (5), 1965-1973 (2008).
6. Velan, S. S., Spencer, R. G. S., Zweier, J. L., & Kuppusamy, P. Electron paramagnetic resonance oxygen mapping (EPROM): Direct visualization of oxygen concentration in tissue. *Magn. Reson. Med.* **43** (6), 804-809 (2000).
7. Elas, M. *et al.* Electron paramagnetic resonance oxygen image hypoxic fraction plus radiation dose strongly correlates with tumor cure in FSA fibrosarcomas. *Int. J. Radiat. Oncol.* **71** (2), 542-549 (2008).
8. Dreher, M. R. *et al.* Nitroxide conjugate of a thermally responsive elastin-like polypeptide for noninvasive thermometry. *Med. Phys.* **31** (10), 2755-2762 (2004).
9. Gallez, B., Mader, K., & Swartz, H. M. Noninvasive measurement of the pH inside the gut by using pH-sensitive nitroxides. An in vivo EPR study. *Magn. Reson. Med.* **36** (5), 694-697 (1996).
10. Halpern, H. J. *et al.* Diminished aqueous microviscosity of tumors in murine models measured with in vivo radiofrequency electron paramagnetic resonance. *Cancer Res.* **59** (22), 5836-5841 (1999).
11. Elas, M., Ichikawa, K., & Halpern, H. J. Oxidative Stress Imaging in Live Animals with Techniques Based on Electron Paramagnetic Resonance. *Radiat. Res.* **177** (4), 514-523 (2012).
12. Kuppusamy, P. *et al.* Noninvasive imaging of tumor redox status and its modification by tissue glutathione levels. *Cancer Res.* **62** (1), 307-312 (2002).
13. Khramtsov, V. V., Yelinova, V. I., Glazachev, Y. I., Reznikov, V. A., & Zimmer, G. Quantitative determination and reversible modification of thiols using imidazolidine biradical disulfide label. *J. Biochem. Biophys. Methods.* **35** (2), 115-128 (1997).
14. Plonka, P. M. Electron paramagnetic resonance as a unique tool or skin and hair research. *Exp. Dermatol.* **18** 472-484 (2009).
15. Halevy, R., Shtirberg, L., Shklyar, M., Blank, A. . Electron Spin Resonance Micro-Imaging of Live Species for Oxygen Mapping. *J. Vis. Exp.* **42** (e122) (2010).
16. Halevy, R., Tormyshev, V., Blank, A. Microimaging of oxygen concentration near live photosynthetic cells by electron spin resonance. *Biophys J.* **99** (3), 971-978 (2010).

17. Eaton, G. R., Eaton, S.S. in *Concepts Magn. Reson.* Vol. 7 49-67 (1995).
18. Maltempo, M. M. Differentiaon of spectral and spatial components in EPR imaging using 2-D image reconstruction algorithms. *J. Magn. Reson.* **69** 156-161 (1986).
19. Tseitlin, M. *et al.* New spectral-spatial imaging algorithm for full EPR spectra of multiline nitroxides and pH sensitive trityl radicals. *J. Magn. Reson.* **245** 150-155 (2014).
20. Mitchell, D. G. *et al.* in *Abstracts of Papers of the American Chemical Society* Vol. 242 (ed Nora Radu Stephen Koch) Denver, CO, (2011).
21. Stoner, J. W. *et al.* Direct-detected rapid-scan EPR at 250 MHz. *J. Magn. Reson.* **170** (1), 127-135 (2004).
22. Tseytlin, M., Biller, J.R., Mitchell, D.G., Yu, Z., Quine, R.W., Rinard, G.A., Eaton, S.S., Eaton, G.R. in *EPR Newsletter.* Vol. 23 8-9 Russian Acaademy of Sciences, Zavoisky Physical-Technical Institute, (2014).
23. Biller, J. R. *et al.* Imaging of nitroxides at 250 MHz using rapid-scan electron paramagnetic resonance. *J. Magn. Reson.* **242** 162-168 (2014).
24. Biller, J. R. *et al.* Improved Sensitivity for Imaging Spin Trapped Hydroxyl Radical at 250 MHz. *Chem. Phys. Chem.* **16** (3), 528-531 (2015).
25. Burks, S. R., Bakhshai, M.A., Makowsky, M.A., Muralidharan, S., Tsai, P., Rosen, G.M., Kao, J.Y. 2H, 15N-Substituted nitroxides as sensitive probes for electron paramagnetic resonance imaging. *J. Org. Chem.* **75** 6463-6467 (2010).
26. Dhimitruka, I., Bobko, A. A., Hadad, C. M., Zweier, J. L., & Khramtsov, V. V. Synthesis and characterization of amino derivatives of persistent trityl radicals as dual function pH and oxygen paramagnetic probes. *J. Am. Chem. Soc.* **130** (32), 10780-10787 (2008).
27. Elajaili, H. B. *et al.* Electron spin relaxation times and rapid scan EPR imaging of pH-sensitive amino-substituted trityl radicals. *Magn. Reson. Chem.* **53** (4), 280-284 (2015).
28. Elajaili, H., Biller, J.R., Rosen, G.M., Kao, J.P.Y., Tseytlin, M., Buchanan, L.B., Rinard, G.A., Quine, R.W., McPeak, J., Shi, Y., Eaton, S.S., Eaton, G.R. Imaging Disulfides at 250 MHz to Monitor Redox Status. *J. Magn. Reson., In Press.* (2015).
29. Tseitlin, M., Rinard, G. A., Quine, R. W., Eaton, S. S., & Eaton, G. R. Deconvolution of sinusoidal rapid EPR scans. *J. Magn. Reson.* **208** (2), 279-283 (2011).
30. Halpern, H. J., Peric, M., Nguyen, T.D., Spencer, D.P., Teicher, B.A., Lin, Y.J., Bowman, M.K. Selective isotopic labeling of a nitroxide spin label to enhance sensitivity for T2 oxymetry. *J. Magn. Reson.* **90** 40-51 (1990).
31. Tsai, P. *et al.* Esters of 5-carboxyl-5-methyl-1-pyrroline N-oxide: A family of spin traps for superoxide. *J. Org. Chem.* **68** (20), 7811-7817 (2003).
32. Biller, J. R. *et al.* Frequency dependence of electron spin relaxation times in aqueous solution for a nitronyl nitroxide radical and perdeuterated-tempone between 250 MHz and 34 GHz. *J. Magn. Reson.* **225** 52-57 (2012).
33. Rosen, G. M. *et al.* Dendrimeric-containing nitronyl nitroxides as spin traps for nitric oxide: Ssynthesis, kinetic, and stability studies. *Macromolecules.* **36** (4), 1021-1027 (2003).
34. Bobko, A. A. *et al.* Redox-sensitive mechanism of no scavenging by nitronyl nitroxides. *Free Radical Biol. Med.* **36** (2), 248-258 (2004).
35. Roshchupkina, G. I. *et al.* In vivo EPR measurement of glutathione in tumor-bearing mice using improved disulfide biradical. *Free Radical Bio. Med.* **45** (3), 312-320 (2008).
36. Mitchell, D. G. *et al.* Use of Rapid-Scan EPR to Improve Detection Sensitivity for Spin-Trapped Radicals. *Biophysical Journal.* **105** (2), 338-342 (2013).
37. Bobko, A. A., Dhimitruka, I., Zweier, J. L., & Khramtsov, V. V. Trityl radicals as persistent dual function pH and oxygen probes for in vivo electron paramagnetic resonance spectroscopy and imaging: Concept and experiment. *J. Am. Chem. Soc.* **129** (23), 7240-+ (2007).
38. Biller, J. R. *et al.* Electron spin-lattice relaxation mechanisms of rapidly-tumbling nitroxide radicals. *J. Magn. Reson.* **236** 47-56 (2013).
39. Redler, G., Barth, E.D., Bauer, K.S., Kao, J.P.Y., Rosen, G.M., Halpern, H.J. In vivo electron paramagnetic resonance imaging of differential tumor targeting using cis-3,4-di(acetoxymethoxycarbonyl)-2,2,5,5-tetramethyl-1-pyrrolidinyloxyl. *Magn. Reson. Med.* **71** (4), 1650-1656 (2013).


 